Materials Today Advances 8 (2020) 100105

Contents lists available at ScienceDirect

Materials Today Advances

journal homepage: www.journals.elsevier.com/materials-today-advances/

Synthesis and characterization of nanocrystalline $U_{1-x}Pu_xO_{2(+y)}$ mixed oxides

G. Kauric [a], O. Walter [b], A. Beck [c], B. Schacherl [c], O. Dieste Blanco [b], J.-F. Vigier [b], E. Zuleger [b], T. Vitova [c, *], K. Popa [b, **]

[a] DEN-Service de la Corrosion et du Comportement des Matériaux dans leur Environnement (SCCME), CEA, Université Paris-Saclay, F-91191, Gif-sur-Yvette, France
[b] European Commission, Joint Research Center, P.O. Box 2340, D-76125, Karlsruhe, Germany
[c] Institut for Nuclear Waste Disposal (INE), Karlsruhe Institute of Technology, P.O. 3640, D-76021, Karlsruhe, Germany

ARTICLE INFO

Article history:
Received 16 June 2020
Received in revised form
29 July 2020
Accepted 29 July 2020
Available online xxx

Keywords:
Hydrothermal decomposition
Oxide nuclear fuel
Oxalate
Plutonium
Uranium
HR-XANES

ABSTRACT

We report here the first synthesis of mixed oxide $U_{1-x}Pu_xO_{2(+y)}$ nanoparticles. The obtained nanopowders were characterized by X-ray diffraction, thermal ionization mass spectrometry, transmission electron microscopy, Raman spectroscopy, and U M_4 edge high-energy-resolution X-ray absorption near edge structure (HR-XANES). The HR-XANES spectra give evidence for the partial oxidation of U^{IV} to U^{V}. This novel route toward the formation of actinide–actinide solid solution opens research opportunities that are not accessible using bulk materials. We give details on the X-ray diffraction study on plutonium oxalate hexahydrate, as a reagent for the synthesis of such nanoparticles.

1. Introduction

Among the different nuclear fuels considered for fast reactors (oxides, carbides, nitrides, and metals), $U_{1-x}Pu_xO_2$ mixed oxide (MOX) with a plutonium content '*x*' over 0.2, is currently the reference fuel. Moreover, in the existing fleet of reactors, MOX fuels are already used but at a lower '*x*' concentration of around 0.07 [1]. Currently, the light water reactor (LWR) MOX fuel is produced by the MIMAS process ('MIcronized MASter blend') [2,3], involving several steps and producing a heterogeneous microstructure [4]. The plutonium dioxide is fabricated by the thermal decomposition of the oxalate (500–800 °C) [5]. However, the products obtained are plate-like agglomerated, which is an issue during the sintering step because of the aggregation and preferential orientation [6].

Recently, Walter et al. [7] developed a method for the synthesis of AnO_2 (*An* = Th, U, Np, Pu) nanocrystals and solid solutions between different tetravalent actinide ions [8,9]. In this method, the conversion of the actinide oxalates is done not thermally, but under hot compressed water (95–250 °C). This technique is fast, close to quantitative and reproducible, suited for the preparation of materials with high purity, homogeneity, and crystallinity. Moreover, it is using only water as reaction and transport medium. This synthesis route gives spheroid-shaped soft agglomerates of nanomaterials, which have a better behavior during sintering [9]. Using this method, Manaud et al. [10] performed a multiparametric study on the UO_2 production and discuss on the uranium oxidation state. To our best knowledge, no nanosized $U_{1-x}Pu_xO_2$ are reported to date, independent on the applied method.

Therefore, in this work, the synthesis of the $U_{1-x}Pu_xO_{2(+y)}$ solid solution with different U-to-Pu ratio has been performed using the hot compressed water decomposition process. The different powders produced were first analyzed by X-ray diffraction (XRD) at room temperature to (i) check their crystallographic purity; (ii) assess the U-to-Pu ratio derived from the Vegard's law; and (iii) evaluate the diameter of the nanocrystals. The uranium-to-plutonium ratio was precisely assessed by thermal ionization mass spectrometry (TIMS). Then, to characterize the structural

* Corresponding author.
** Corresponding author.
E-mail addresses: tonya.vitova@kit.edu (T. Vitova), karin.popa@ec.europa.eu (K. Popa).

https://doi.org/10.1016/j.mtadv.2020.100105

properties of the prepared mixed oxide fuels, the nanocrystals were analyzed by U M_4 high-energy-resolution X-ray absorption near edge spectroscopy (HR-XANES), transmission electron microscopy (TEM), and Raman spectroscopy. In addition, we report the XRD study on plutonium oxalate hexahydrate, which is an intermediate compound in the synthesis of plutonium dioxide nanopowder.

2. Experimental

2.1. Synthesis

^{238}U is an α-emitter (half-life: 4.47 billion years), which is only weakly radioactive. However, we used a plutonium batch (^{239}Pu main isotope) containing about 2% of ^{241}Am, which is a highly radioactive material. Because of the potential health risk, we handled the material in a properly regulated and controlled radiological facility.

2.1.1. Plutonium oxalate hexahydrate

Plutonium oxalate has been synthesized and characterized along this study as a model for the $(U_{1-x}Pu_x)(C_2O_4)_2 \cdot nH_2O$ solid solutions. Even if the production of this compound is trivial and known since many decades, its structure was not determined because of technical difficulties (partial dehydration during measurements). Thus, a Pu^{IV} solution (0.2 M in 4 M HNO_3 and 0.04 M HF) was precipitated with an excess of $C_2O_4H_2$ solution (0.8 M in 1 M HNO_3) at room temperature under continuous stirring. The precipitate was filtered under vacuum and washed several times with deionized water.

$$Pu^{4+} + 2C_2O_4H_2 + 6H_2O \rightarrow Pu(C_2O_4)_2 \cdot 6H_2O + 4H^+$$

As the obtained hydrated oxalate is unstable and rapidly dehydrates partially at room temperature, a sample of the obtained oxalate still slightly wet after filtration has been taken for XRD analysis. About 10 mg of the wet powder was embedded in an epoxy resin to slow down the dehydration process. The mixture was then fixed on the XRD sample holder.

2.1.2. Preparation of mixed dioxides

For the synthesis of the $U_{1-x}Pu_xO_{2(+y)}$ nanocrystals, we used a method based on hydrothermal decomposition of mixed oxalates at low temperature, as described elsewhere [7]. In short, solutions of U^{IV} (0.5 M, obtained by electroreduction of $UO_2(NO_3)_2$ solution in 8 M HNO_3, depleted uranium) and Pu^{IV} (0.8 M in 4 M HNO_3, plutonium vector of ^{239}Pu main isotope, containing 2% ^{241}Am) were mixed in the 94:6, 88:12, 75:25, and 60:40 U:Pu (mol%) ratio. The mixed oxalate $(U_{1-x}Pu_x)(C_2O_4)_2 \cdot nH_2O$ was obtained by direct coprecipitation of the U^{IV} and Pu^{IV} solutions in nitric acid adding an excess of 1 M solution of oxalic acid [11–14]. The obtained precipitate was washed several times with distilled water to remove any trace of nitrate, which induces the oxidation of U^{IV} to soluble U^{VI} under the working temperature conditions.

The decomposition of the oxalates has been performed in a 25-mL Teflon-lined hydrothermal synthesis autoclave reactor. The thermal treatments were performed using a heating mantel preheated at the required temperature while the temperature was controlled by thermocouples. Compared to the usual oxalates decomposition by calcination, this method uses temperature and pressure to achieve the conversion into oxide. A small amount of water (5 mL) is added to the powder and the obtained suspension is mixed by stirring. Hence, by heating above the boiling point of water (200 °C for MOX-6, MOX-13, and MOX-29; 220 °C for MOX-46), the water vaporizes and the pressure increases in the autoclave (also due to the gaseous CO and CO_2 formed by decomposition). After a reaction time of 4 h, under autogenic pressure (calculated to be of 25–30 bar), the resulting nanocrystals were washed with water, ethanol, and acetone, to gradually decrease the polarity of the solution. The work was performed under nitrogen and using minute amounts of hydrazine, in order to limit the oxidation of U^{IV}.

2.2. Powder X-ray diffraction

Room temperature XRD analyses were performed on a Bruker D8 diffractometer mounted in a Bragg–Brentano configuration with a curved Ge (1,1,1) monochromator and a ceramic copper tube (40 kV, 40 mA) and supplied with a LinxEye position sensitive detector. The data were collected by step scanning in the angle range $10° \leq 2\theta \leq 120°$, with a step size of 0.008° (2θ); total measuring time was about 8 h.

2.3. Transmission electron microscopy

The samples were analyzed by TEM using a TecnaiG2 (FEI™) 200 kV microscope equipped with a field emission gun, modified during its construction to enable the examination of radioactive samples. They were prepared by dropping suspended samples on a TEM grid and evaporating the solvent. TEM images have been recorded using a Gatan US1000 slowscan CCD camera. Electron energy loss spectroscopy (EELS) has been used to estimate the uranium-to-plutonium ratio of the samples.

2.4. Isotope dilution thermal ionization mass spectrometry

A sample of 20 mg for each composition was dissolved in nitric acid. The elemental content of uranium and plutonium was measured by thermal ionization mass spectroscopy, adding a known amount of a solution containing the element to be investigated. Certified isotope standards are used as reference materials provided from accredited institutes such as EC-JRC (Belgium) or CETAMA (France) [15].

2.5. Raman spectroscopy

Raman measurements were carried out on the polycrystalline samples at room temperature using a Horiba Jobin-Yvon T64000 spectrometer with a 647 nm Kr+ laser excitation source. A 50× objective was used to irradiate the sample and collect the backscattered light. Measurements were carried out at 4–10 mW incident power. However, to drop the fluorescence of the samples, they were shortly irradiated at higher laser power just before measurement.

2.6. U M_4 HR-XANES

U M_4 absorption edge HR-XANES spectroscopy technique was conducted at the ACT station of the CAT-ACT-Beamline for catalysis and actinide research of the KIT synchrotron light source facility, Karlsruhe, Germany. A detailed description of the beamline is reported by Zimina et al. [16] The incident beam was vertically collimated by a bare Si mirror and monochromatized by a double crystal monochromator (DCM) equipped with Si(111) crystals and focused to 500 × 500 μm^2 onto the sample by a toroidal, double-focusing Si-mirror. The DCM was calibrated by assigning 3,725.5 eV to the maximum of the most intensive absorption resonance (white line, WL) of the U M_4 edge HR-XANES spectrum of the UO_2 reference sample. The uncertainty in the energy positions of the spectral features is estimated to be about ±0.05 eV, corresponding to half of the energy step size.

The HR-XANES spectra were obtained using a Johann-type multianalyzer crystal X-ray emission spectrometer. The sample, crystals, and a single diode VITUS silicon drift detector (KETEK, Germany) were arranged in a vertical Rowland circle geometry. The U M_4 HR-XANES spectra were obtained by recording the U M_β emitted fluorescence as a function of the incident energy. The emission energy was selected using the 220 reflection of four spherically bent Si(110) analyzer crystals (Saint-Gobain, France) with a bending radius of 1 m, aligned at a Bragg angle of 75.36°. The crystals were covered with masks with 50 mm diameter, which improved the experimental resolution. The size of the incident beam on the sample was defined by a slit with 500 × 500 μm^2 size, which additionally improved the experimental energy resolution. The U M_4 HR-XANES spectra were measured within 3,710–3,900 eV energy region. The step size was 0.1 eV within 3,720–3,740 eV and 0.5 eV in all other parts of the spectra; two spectra were averaged for each sample. The sample, crystals, and detector were enclosed in a box filled with He to minimize intensity losses due to scattering and absorption of photons in air. Constant He flow was maintained to keep the O level ≤0.1%. No radiation damage was observed during the measurements. The UO_2 reference is a quarter of a ceramic $^{238}UO_2$ pellet with thickness of 1 mm and mass of 50 mg. The pellet was heated for 6 h at 1,150 °C in H_2/Ar-flow (8% H_2) and enclosed in two containments with windows consisting Kapton foil with thickness 8 and 13 μm. As the sample is stored under air some oxidation to UO_{2+y} on the surface is expected.

The $U_{1-x}Pu_xO_{2(+y)}$ samples were placed in a multiposition plexiglass sample holder with 8 μm thickness of the Kapton windows, thereby double containment (inner and outer) of the samples was achieved. About 100 μg of sample was mixed with 10 mg bicomponent glue and placed in the inner cells.

3. Results and discussion

3.1. Plutonium oxalate hexahydrate

Structural refinement could not be performed in the given experimental condition, but a Rietveld refinement of the data was done by fixing atomic position (Table 1) to the ones determined for $U(C_2O_4)_2 \cdot 6H_2O$ compound [17]. The plutonium oxalate shows a monoclinic symmetry, in space group *C*2/*m*. The refined cell parameters are reported on Fig. 1. The good correlation obtained between experimental and calculated data confirmed the formation of a pure Pu^{IV} oxalate hexahydrate having the same structure of the uranium analogue.

Lattice parameter variation of the oxalate hexahydrate in the *C*2/*m* monoclinic structure is presented in the Table 2. One can observe as expected the contraction of the structure as a function of actinide ionic radii reduction. The contraction is specially marked for the *a* and *b* parameter, i.e., within the oxalate layer, and more moderately affected on the *c* parameter, i.e., on the oxalate interlayer separation.

Table 1
Atomic positions used for $Pu(C_2O_4)_2 \cdot 6H_2O$ Rietveld refinement, based on Duvieubourg-Garela et al. [17] structural determination.

Atom	Wyck.	Site	*x*/*a*	*y*/*b*	*z*/*c*	U [Å^2]
Pu1	2a	2/*m*	0	0	0	0.01
C1	8j	1	0.255	0.247	0.099	0.01
O1	8j	1	0.174	0.162	0.171	0.01
O2	8j	1	0.352	0.333	0.163	0.01
O3	4h	2	1/2	0.217	1/2	0.01
O4	4i	M	0.716	0	0.486	0.01
O5	2b	2/*m*	0	1/2	0	0.01
O6	2c	2/*m*	1/2	1/2	1/2	0.01

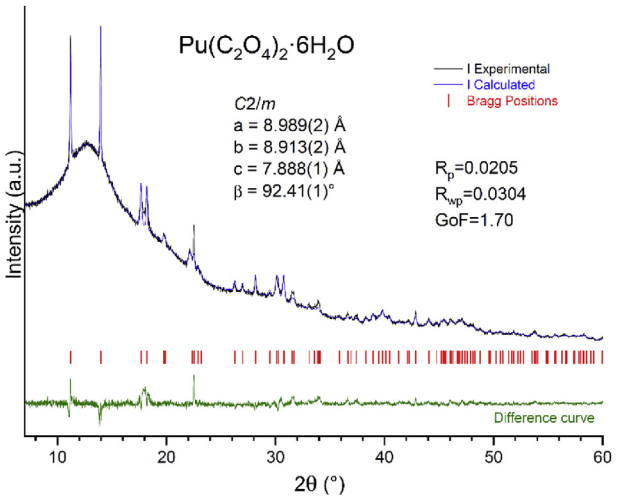

Fig. 1. Rietveld refinement of $Pu(C_2O_4)_2 \cdot 6H_2O$. Atomic positions were fixed to the values presented in Table 2. The high background is due to the sample preparation method (powder embedded in epoxy resin), done to prevent oxalate dehydration.

3.2. $U_{1-x}Pu_xO_2$ nanocrystals

3.2.1. XRD, TEM, and TIMS

After the hot-compressed water decomposition treatment of the oxalates, the formed nanocrystals of $U_{1-x}Pu_xO_{2(+y)}$ show a fluorite-type cubic structure, crystalizing in the *Fm*-3*m* (225) space group. The collected XRD patterns are reported in Fig. S1, and no additional peaks were found. The refined cell parameters obtained from the Rietveld refinement of the XRD data are reported in Table 3. In the same table, we report the crystallite sizes of each composition, calculated using the full width at half maximum of at least six selected peaks in the 2θ range between 25° and 100° and measured with TEM.

To determine the ratio U to Pu of the different theoretical compositions, we carried out a TIMS measurement, also reported in Table 3 (details in Table S1).

The plutonium content for each sample measured by ID-TIMS is in good agreement with the expected values. The cell parameters refined for each sample are also in good agreement with Vegard's law. It is apparent in Fig. 2 that for the MOX-13 and MOX-29, there is a slight deviation from the ideal lattice constant, indicating a partial oxidation of the samples.

The TEM analysis reported in Fig. 3 shows that the nanocrystals are attached to each other forming agglomerates as it has been observed by Popa et al. [8] and Balice et al. [9] for other systems. For the mixed oxide with MOX-29, the sizes of the agglomerates are between 175 and 350 nm. Moreover, the diameter of the particles was determined and reported in Table 3. For the MOX-13, MOX-29, and MOX-46, the samples seemed to be formed from only one size of particles, whereas for the MOX-6 two families of particles have been observed. One has an average size of 11 ± 3 nm that fits well with the crystallite size derived from the XRD pattern analysis. The other one has a larger diameter of an average of 55 ± 18 nm (Fig. 3a). For the three other compositions, there is a good agreement between the two techniques. The ratios U:Pu observed in the different-sized nanocrystals did not change substantially to suggest heterogeneity. Due to limitations on the spot size of our setup in scanning transmission electron microscopy (STEM) mode, EELS has

Table 2
Lattice parameter comparison between, $U(C_2O_4)_2 \cdot 6H_2O$, $Np(C_2O_4)_2 \cdot 6H_2O$, and $Pu(C_2O_4)_2 \cdot 6H_2O$.

Reference		*a* [Å]	*b* [Å]	*c* [Å]	*β* [°]	*V* [Å^3]	An^{4+} radii CN8
Duvieubourg-Garela et al. [17]	U	9.0953	8.9896	7.9046	92.212	645.82	1.00
Grigoriev et al. [18]	Np	9.028	8.952	7.867	92.61	635.14	0.98
This study	Pu	8.989	8.913	7.888	92.41	631.42	0.96

Table 3
Cell parameters and crystallite sizes obtained from the XRD and TEM results for the different compositions of mixed oxide fuel nanocrystals synthesized.

Composition	*a* (Å)	*d* (nm) XRD	*d* (nm) TEM	Reference	Notation
UO_2	5.470 (1)	5.5 ± 0.5	–	[7]	
$U_{0.942}Pu_{0.058}O_2$	5.463 (2)	14 ± 2	11 ± 3/55 ± 18	This work	MOX-6
$U_{0.874}Pu_{0.126}O_2$	5.452 (3)	9 ± 1.8	12 ± 3	This work	MOX-13
$U_{0.707}Pu_{0.293}O_2$	5.442 (2)	7 ± 1.4	7 ± 2	This work	MOX-29
$U_{0.54}Pu_{0.46}O_2$	5.436 (1)	19 ± 3	33 ± 12	This work	MOX-46
PuO_2	5.397 (1)	3.6 ± 0.3	–	[7,19]	

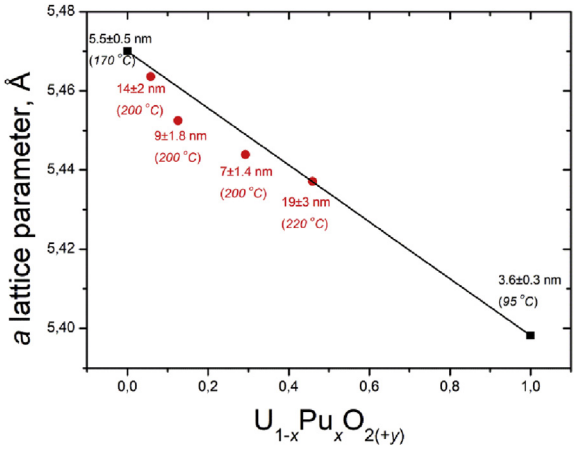

Fig. 2. Evolution of the lattice parameter of $U_{1-x}Pu_xO_{2(+y)}$ solid solutions as a function of the substitution degree. The lattice parameter values are taken from Refs. [7,19], respectively.

been used to calculate these ratios locally; again, the observations did not yield to a determination of inhomogeneity on the sample.

To assess the stability of the nanopowder at 800 °C, an annealing of 20 h under argon atmosphere has been done for the MOX-29 sample. The XRD pattern after thermal treatment is similar to the one before annealing (see Fig. S3), with increased crystallinity and with a slight increase of the lattice parameter up to 5.444 (1) Å. After annealing, we obtained a diameter of 33 ± 10 nm, which is in good agreement with the TEM measurements (Fig. S4). Moreover, it follows the trend observed by Popa et al. [8] for the end members, who obtained for UO_2 at 800 °C, a crystallite size around 50 nm and for PuO_2 of circa 20 nm.

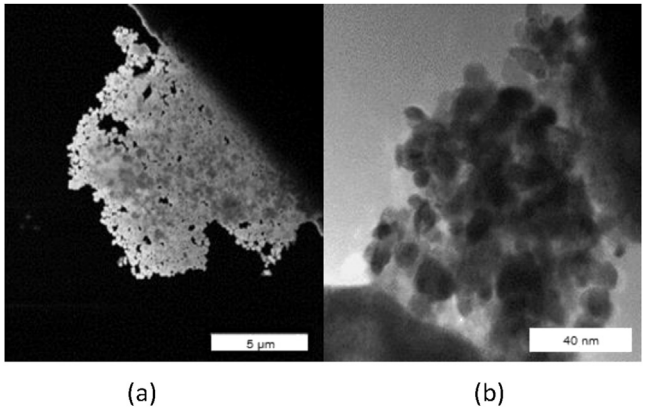

Fig. 3. Transmission electron micrographs of nanocrystalline MOX-29 sample. In (a), an agglomerate of nanocrystals has been observed; (b) shows a zoom on an agglomerate where nanocrystals can be better observed.

3.2.2. HR-XANES

The actinide (*An*) $M_{4,5}$ edge HR-XANES technique probes mainly the *An* unoccupied *f*-density of states in presence of a core-hole in the intermediate ($3d^9 4f^{14} 5f^{n+1}$) and final state ($3d^{10} 4f^{13} 5f^{n+1}$) of the absorption process [20–22]. At the *An* M_4 absorption edge, the predominant electronic transitions are $3d_{3/2} \rightarrow 5f_{5/2}$ followed by $4f_{5/2} \rightarrow 3d_{3/2}$ emission of M_β characteristic fluorescence (dipole selection rule $\Delta J = 0, \pm 1$). Since the 5f valence electrons of U participate in the chemical bonding, changes of electronic structure due to variation of oxidation states and/or atomic environments of the U atoms will be reflected in the U M_4 edge HR-XANES spectrum. The U M_4 HR-XANES method mainly probes the bulk of the material and can detect a small amount of one actinide oxidation state in mixtures. One prominent example for *An*-speciation analyses is the ability to clearly resolve U^V when it is mixed with U^{IV} [21,23,24].

Fig. 4 depicts the U M_4 edge HR-XANES spectra of the three MOX-X (X = 6, 13, 29) compounds synthesized following the same

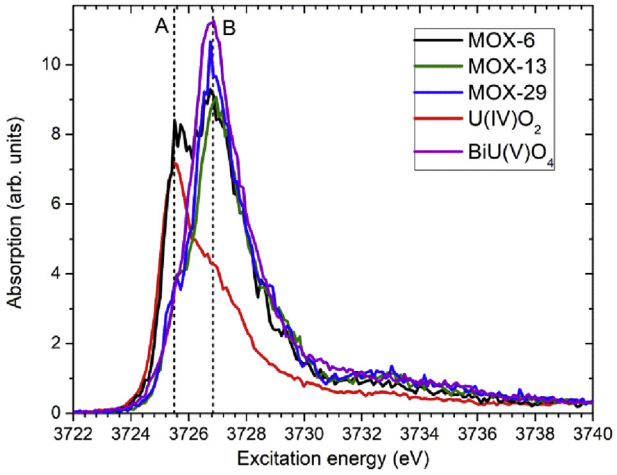

Fig. 4. U M_4 HR-XANES spectra of the MOX-6, MOX-13, and MOX-29 samples and the BiU^VO_4 and UO_2 references. Lines A and B mark the peaks characteristic for U^{IV} and U^V.

experimental conditions compared with the bulk $U^{IV}O_2$ and $BiU^{V}O_4$ references. The post edge regions of the U M_4 edge spectra are depicted in Fig. S6. The use of an X-ray emission spectrometer allows to select only the U M_β and to filter out the Pu M_α characteristic fluorescence; those emission lines overlap and are not possible to separate when a conventional solid-state detector is applied. However, the spectral intensity abruptly decreases at about 3,778.5 eV when the Pu M_5 edge is approached (cf. Fig. S6). The cross section for absorption of photons by Pu atoms increases at this energy. As a result, less photons are absorbed by U resulting in the decrease of the intensity of the emitted fluorescence. The size of this dip in the spectra implies that the relative amount of Pu in the samples increases as follows: MOX-6 < MOX-13 < MOX-29 as found also by TIMS.

The bulk UO_2 reference contains predominantly U^{IV} and a small amount of U^{V} due to surface oxidation of UO_2 kept in air [21,25]. This is visible in Fig. 4 since the UO_2 spectrum has a pronounced shoulder on the high energy side of the main absorption peak marked with line B. The energy position of line B is characteristic of the main absorption intensity of U^{V} substituting U^{IV} in the cubic structure of UO_2, i.e., UO_{2+y} [21,23]. Note that, the spectrum of a U^{IV} compound, which does not contain U^{V} also has a feature at this energy position but with much lower intensity. We showed previously that $BiU^{V}O_4$ contains U^{V} in a fluorite structure (*Fm*-3*m*) similar to U^{IV}/U^{v} in UO_2/UO_{2+y}; therefore, it is a very suitable U^{V} reference compound [24]. The main absorption peak of the spectrum of $BiU^{V}O_4$ is also located at the energy position of line B. The U M_4 edge HR-XANES spectra of MOX-29 and MOX-13 are very similar, whereas the spectrum of MOX-6 differs.

The spectra contain characteristic peaks for U^{IV} (line A) and U^{V} (line B), which are about 1.1 eV apart. U^{V} dominates in the MOX-29 and MOX-13 samples. U^{V} and U^{IV} have comparable contributions in MOX-6. The smaller particles size of MOX-29 and MOX-13 (7 and 9 nm, respectively) compared to MOX-6 (14 nm) (cf. Table 3) leads to larger surface area; hence we assume that more U atoms oxidize from U^{IV} to U^{V} on the surface of the particles. This assumption is based on the correlation between the decreases of the size of the particles and the increase of the U^{v} content revealed by the U M_4 edge HR-XANES spectra. Note that, quantitative analyses like linear combination least squares fit analyses are not recommendable since the areas of the spectral peaks of the U M_4 edge HR-XANES spectra can deviate from the absorption cross sections of the different U oxidation states thus we do not attempt them here [26].

Another contribution to the uranium oxidation from IV to V is given by the presence of about 2% of americium in the original plutonium vector; thus, the MOX-46 would contain close to 1% Am out of the total of the actinides in the sample. It has been shown that substitution of tetravalent uranium with trivalent ions such as americium is compensated by the oxidation of U^{IV} to U^{V} [27]. Moreover, charge compensation in the Am/Pu system is also possible [28] and cannot be excluded at this stage.

4. Conclusions and perspectives

We present here the synthesis of nanometric mixed oxides $U_{1-x}Pu_xO_{2(+y)}$ with different plutonium content as homogeneous fuels for fast reactors. The newly developed method of oxalate decomposition under hot compressed water at low temperature has several advantages, allowing sintering compared with the thermal conversion of oxalates. This preparation method provides particles with spheroid shape and small size, in contrast to the plate-like morphology previously achieved by thermal decomposition. The U M_4 HR-XANES spectra provide evidence for oxidation of U^{IV} to U^{V} in the $U_{1-x}Pu_xO_{2(+y)}$ nanocrystals.

The method is promising for low temperature production of mixed oxides powders and opens research opportunities which are not accessible using bulk materials. Such materials are proven to be very reactive, hence smoothing the path for solid-state synthesis of different compounds of interest for accident case scenario, such as sodium uranoplutonates. There are used as standards to study the environmental dispersion of nuclear materials [29]. Finally, the accommodation of an important amount of americium in the samples rich in plutonium is the first indication that the method is suitable for production of homogeneous transmutation fuels.

Accession codes

CCDC 1999798 contains the supplementary crystallographic data for this paper.

Data availability statement

The raw/processed data required to reproduce these findings cannot be shared at this time due to technical or time limitations.

Credit author statement

G.K. Investigation (synthesis, sample preparation, transport, XRD, HR-XANES). Writing – original draft. Visualisation.

O.W. Conceptualisation. Methodology. Investigation (sample preparation, transport, HR-XANES). Visualisation.

A.B. Investigation (HR-XANES). Writing – original draft. Visualisation.

B.S. Investigation (HR-XANES). Visualisation.

O.D.B. Investigation (TEM). Visualisation.

J.F.V. Investigation (synthesis, XRD). Formal analysis. Writing – original draft. Visualisation.

E.Z. Investigation (managing the analytical service). Formal analysis. Visualisation.

T.V. Conceptualisation. Investigation (HR-XANES). Formal analysis. Writing – original draft. Writing – review and editing. Visualisation. Supervision.

K.P. Conceptualisation. Methodology. Investigation (synthesis, sample preparation, transport). Formal analysis. Writing – original draft. Writing – review and editing. Visualisation. Supervision.

Declaration of competing interest

The authors declare that they have no known competing financial interests or personal relationships that could have appeared to influence the work reported in this paper.

Acknowledgments

G.K. acknowledges support from the ENEN+ project (EURATOM Research and Training programme H2020 No. 755576). T.V. A.B. and B.S. acknowledge the Helmholtz Association of German Research Centers for the VH-NG-734 grant. The authors acknowledge the Institute of Beam Physics and Technology (IBPT) for the operation of the storage ring, the Karlsruhe Research Accelerator (KARA) and the Analytical Service of JRC-Karlsruhe for ID-TIMS measurements. The technical support of Daniel Bouëxière (XRD), Jean-Yves Colle (Raman), and Antony Guiot (samples production) is highly appreciated. Rudy Konings and Roberto Caciuffo are acknowledged for their valuable advice. The authors thank Steliyana Lehchanska for the design of the graphical abstract art.

Appendix ASupplementary data

Supplementary data to this article can be found online at https://doi.org/10.1016/j.mtadv.2020.100105.

References

[1] J.-L. Provost, M. Debes, MOX and UOX PWR fuel performances EDF operating experience, J. Nucl. Sci. Technol. 43 (2006) 960–962.

[2] D. Haas, A. Vandergheynst, J. van Vliet, R. Lorenzelli, J.-L. Nigon, Mixed-oxide fuel fabrication technology and experience at the Belgonucléaire and CFCa plants and further developments for the MELOX plant, Nucl. Technol. 106 (1994) 60–82.

[3] R. Liberge, M.-H. Mouliney, S. Masson, J.-C. Thieblemont, The French experience in dry milling of nuclear ceramic powders, in: WM'99 Conference, February 28 - March 04, 1999.

[4] Z. Talip, S. Peuget, M. Magnin, M. Tribet, C. Valot, R. Vauchy, C. Jégou, Characterization of un-irradiated MIMAS MOX fuel by Raman spectroscopy and EPMA, J. Nucl. Mater. 499 (2018) 88–97.

[5] R.M. Orr, H.E. Sims, R.J. Taylor, A review of plutonium oxalate decomposition reactions and effects of decomposition temperature on the surface area of the plutonium dioxide product, J. Nucl. Mater. 465 (2015) 756–773.

[6] V. Tyrpekl, J.-F. Vigier, D. Manara, T. Wiss, O. Dieste Blanco, J. Somers, Low temperature decomposition of U(IV) and Th(IV) oxalates to nanograined oxide powders, J. Nucl. Mater. 460 (2015) 200–208.

[7] O. Walter, K. Popa, O. Dieste Blanco, Hydrothermal decomposition of actinide(IV) oxalates: a new aqueous route towards reactive actinide oxide nanocrystals, Open Chem 14 (2016) 170–174.

[8] K. Popa, O. Walter, O. Dieste Blanco, A. Guiot, D. Bouëxière, J.-Y. Colle, L. Martel, M. Naji, D. Manara, A low-temperature synthesis method for AnO_2 nanocrystals (An = Th, U, Np, and Pu) and associate solid solutions, CrystEngComm 20 (2018) 4614–4622.

[9] L. Balice, D. Bouëxière, M. Cologna, A. Cambriani, J.-F. Vigier, E. De Bona, G.D. Sorarù, C. Kübel, O. Walter, K. Popa, Nano and micro $U_{1-x}Th_xO_2$ solid solutions: from powders to pellets, J. Nucl. Mater. 498 (2018) 307–313.

[10] J. Manaud, J. Mayanadié, A. Mesbah, M.O.J.Y. Hunault, P.M. Martin, M. Zunino, D. Meyer, N. Dacheux, N. Clavier, Hydrothermal conversion of uranium(IV) oxalate into oxides: a comprehensive study, Inorg. Chem. 59 (2020) 3260–3273.

[11] N. Clavier, N. Hingant, M. Rivenet, S. Obbade, N. Dacheux, N. Barré, F. Abraham, X-ray diffraction and μ-Raman investigation of the monoclinic-orthorhombic phase transition in $Th_{1-x}U_x(C_2O_4)_2{\cdot}2H_2O$ solid solutions, Inorg. Chem. 49 (2010) 1921–1931.

[12] F. Abraham, B. Arab-Chapelet, M. Rivenet, C. Tamain, S. Grandjean, Actinide oxalates, solid state structures and applications, Coord. Chem. Rev. 266–267 (2014) 28–68.

[13] C. Tamain, B. Arab-Chapelet, M. Rivenet, X.F. Legoff, G. Loubert, S. Grandjean, F. Abraham, Coordination modes of americium in the $Am_2(C_2O_4)_3(H_2O)_6{\cdot}4H_2O$ oxalate: synthesis, crystal structure, spectroscopic characterizations and comparison in the $M_2(C_2O_4)_3(H_2O)_6{\cdot}nH_2O$ (M = Ln, An) series, Inorg. Chem. 55 (2016) 51–61.

[14] C. Tamain, B. Arab-Chapelet, M. Rivenet, S. Grandjean, F. Abraham, Crystal growth methods dedicated to low solubility actinide oxalates, J. Solid State Chem. 236 (2016) 246–256.

[15] C. Andor, Work Instruction WI0214/S5/R4, Determination of Uranium and Plutonium Isotopic Content and Concentration in Nitric Acid Solutions by Thermal Ionization Mass Spectrometry Using the Total Evaporation Technique, JRC Karlsruhe, 2014.

[16] A. Zimina, K. Dardenne, M.A. Denecke, D.E. Doronkin, E. Huttel, H. Lichenberg, S. Mangold, T. Pruessmann, J. Rothe, T. Spangenberg, S. Steininger, T. Vitova, H. Geckeis, J.-D. Grunwaldt, CAT-ACT-A new highly versatile X-ray spectroscopy beamline for catalysis and radionuclide science at the KIT synchrotron light facility ANKA, Rev. Sci. Instrum. 88 (2017) 113113.

[17] L. Duvieubourg-Garela, N. Vigier, F. Abraham, S. Grandjean, Adaptable coordination of U(IV) in the 2D-(4,4) uranium oxalate network: from 8 to 10 coordinations in the uranium (IV) oxalate hydrates, J. Solid State Chem. 181 (2008) 1899–1908.

[18] M.S. Grigoriev, I.A. Charushnikova, N.N. Krot, A.I. Yanovskii, Y.T. Struchkov, Crystal structure of the neptunium(IV) oxalate hexahydrate $Np(C_2O_4)_2{\cdot}6H_2O$, Radiochemistry 39 (1997) 419–425.

[19] D. Bouëxière, K. Popa, O. Walter, M. Cologna, Kinetic study on the grain growth of PuO_2 nanocrystals, RSC Adv. 9 (2019) 6542–6547.

[20] T. Vitova, I. Pidchenko, D. Fellhauer, P.S. Bagus, Y. Joly, T. Pruessmann, S. Bahl, E. Gonzalez-Robles, J. Rothe, M. Altmaier, M.A. Denecke, H. Geckeis, The role of the 5f valence orbitals of early actinides in chemical bonding, Nat. Commun. 8 (2017) 16053.

[21] K.O. Kvashnina, S.M. Butorin, P. Martin, P. Glatzel, Chemical state of complex uranium oxides, Phys. Rev. Lett. 111 (2013) 253002.

[22] T. Vitova, M.A. Denecke, J. Göttlicher, K. Jorissen, J.J. Kas, K. Kvashnina, T. Prüßmann, J.J. Rehr, J. Rothe, Actinide and lanthanide speciation with high-energy resolution X-ray techniques, J. Phys. 430 (2013), 012117.

[23] I. Pidchenko, K.O. Kvashnina, T. Yokosawa, N. Finck, S. Bahl, D. Schild, R. Polly, E. Bohnert, A. Rossberg, J. Gottlicher, K. Dardenne, J. Rothe, T. Schafer, H. Geckeis, T. Vitova, Uranium redox transformations after U(VI) coprecipitation with magnetite nanoparticles, Environ. Sci. Technol. 51 (2017) 2217–2225.

[24] K. Popa, D. Prieur, D. Manara, M. Naji, J.-F. Vigier, P.M. Martin, O. Dieste Blanco, A.C. Scheinost, T. Prüßmann, T. Vitova, P.E. Raison, J. Somers, R.J.M. Konings, Further insights into the chemistry of the Bi-U-O system, Dalton Trans. 45 (2016), 7847-5855.

[25] S.B. Donald, M.L. Davisson, Z. Dai, S.K. Roberts, A.J. Nelson, Relative impact of H_2O and O_2 in the oxidation of UO_2 powders from 50 to 300 C, J. Nucl. Mater. 496 (2017) 353–361.

[26] T. Vitova, I. Pidchenko, D. Schild, T. Prüßmann, V. Montoya, D. Fellhauer, X. Gaona, E. Bohnert, J. Rothe, R.J. Baker, H. Geckeis, Competitive reaction od neptunium(V) and uranium(VI) in potassium-sodium carbonate-rich aqueous media: speciation study with a focus on high-resolution X-ray spectroscopy, Inorg. Chem. 59 (2020) 8–22.

[27] S.M. Butorin, K.O. Kvasnina, D. Prieur, M. Rivenet, P.M. Martin, Characteristics of chemical bonding of pentavalent uranium in La-doped UO_2, Chem. Commun. 53 (2016) 115–118.

[28] E. Epifano, M. Naji, D. Manara, A.C. Scheinost, C. Hening, J. Lechelle, R.J.M. Konings, C. Guéneau, D. Prieur, T. Vitova, K. Dardenne, J. Rothe, P.M. Martin, Extreme multi-valence states in mixed actinides oxides, Commun. Chem. 2 (59) (2019) 1–11.

[29] J.-Y. Colle, S. Stohr, B. Cremer, S. Van Winckel, G. Rasmussen, O. Dieste Blanco, T. Wiss, R.J.M. Konings, Uranium-plutonium partitioning in aerosols produced from $(U,Pu)O_2$ mixed oxides by laser heating, J. Aerosol. Sci. 148 (2020) 105588, 1-13.